Measuring the scrambling of quantum information

Brian Swingle,[1,2,*] Gregory Bentsen,[1] Monika Schleier-Smith,[1] and Patrick Hayden[1,2]

[1] *Department of Physics, Stanford University, Stanford, California 94305, USA*
[2] *Stanford Institute for Theoretical Physics, Stanford, California 94305, USA*

We provide a protocol to measure out-of-time-order correlation functions. These correlation functions are of theoretical interest for diagnosing the scrambling of quantum information in black holes and strongly interacting quantum systems generally. Measuring them requires an echo-type sequence in which the sign of a many-body Hamiltonian is reversed. We detail an implementation employing cold atoms and cavity quantum electrodynamics to realize the chaotic kicked top model, and we analyze effects of dissipation to verify its feasibility with current technology. Finally, we propose in broad strokes a number of other experimental platforms where similar out-of-time-order correlation functions can be measured.

arXiv:1602.06271v1 [quant-ph] 19 Feb 2016

Ongoing advances in the coherent manipulation of quantum many-body systems have enabled experimental measurements of the dynamics of quantum information [1–4]. For example, recent experiments [1] have corroborated the Lieb-Robinson bound, a fundamental speed limit on the propagation of signals even in non-relativistic spin systems [5]. At the same time, new theoretical bounds on the dynamics of entanglement have been derived from the study of black holes [6]. Consistent with their wide variety of extreme physical properties, black holes often saturate absolute limits on quantum information processing. They are the densest memories in nature [7]. They also process their information extremely rapidly [8, 9] and reach the maximal rate of growth of chaos [10].

That black holes process quantum information at all is demonstrated by the holographic principle [11, 12] and AdS/CFT duality: a black hole in asymptotically anti-de Sitter space is equivalent to a thermal state of a lower dimensional quantum field theory *without gravity* [13]. This means that certain ordinary quantum mechanical systems [14, 15], of a type that could in principle be realized in experiments, e.g. [16], are dynamically equivalent to black holes in quantum gravity. A major open question is the extent to which familiar quantum many-body systems also behave like black holes. To make progress on this question, this article focuses on a particular process known as scrambling, in which quantum information in a localized perturbation is spread across a quantum many-body system's degrees of freedom and thereby made inaccessible to local measurements. Our broader motivations are the desire to understand fundamental limits on quantum information processing and the prospect of experimental tests (or quantum simulations) of the holographic principle and quantum gravity.

Black holes are conjectured to be the fastest scramblers in nature [9], so it useful to recall how the notion of scrambling first appeared in the black hole context. Consider a 3+1 dimensional Schwarzchild black hole of radius $R = 2GM$ in flat space (G is Newton's constant and M is the mass. The speed of light and Boltzmann's constant are set to one.) Now suppose we perturb the black hole. The equilibration time τ is determined by the imaginary part of the vibrational frequencies of the black hole. R is the only length scale in the problem, so τ must be proportional to R, but it is illuminating to recast this timescale in terms of the black hole's temperature $T = \frac{\hbar}{8\pi GM}$ [17]. The equilibration timescale is then $\tau = \frac{\hbar}{2\pi T}$, the basic timescale of a finite-temperature quantum system.

The microscopic dynamics of the black hole remain nontrivial even after macroscopic equilibrium is reached: quantum information in the perturbation continues to be swept up, or scrambled, into a more complex global form. The black hole's entropy, $S_{\rm BH} = \frac{4\pi R^2}{4\hbar G}$, is taken to define the effective number degrees of freedom, the number of qubits. Then a toy model of the black hole dynamics in which at each time step random pairs of qubits interact predicts a global scrambling time for quantum information given by $t_* = \tau \log S_{\rm BH}$ [8]. Intuitively, if at each time step τ, each of the $S_{\rm BH}$ qubits interacts with one other qubit, then the information in one qubit rapidly spreads to 2, 4, ... $2^{t/\tau}$ qubits. After a time $\tau \log S_{\rm BH}$, the information in a single qubit is spread over the entire system, providing an estimate of t_*.

Recent work on chaos and black holes [6, 18] has shown that out-of-time-order correlation functions, similar in spirit to echo measurements [19], give access to the scrambling time t_*. Given two commuting unitary operators V and W and a time evolution operator $U(t) = e^{-iHt}$ (setting $\hbar = 1$), the four point out-of-time-order correlator is $F(t) = \langle W_t^\dagger V^\dagger W_t V\rangle$, where $W_t = U(-t)WU(t)$ is the Heisenberg operator. For black holes in Einstein gravity, the out-of-time-order equilibration time is $\tau \log S_{\rm BH}$ [6], the same as the information theoretic scrambling time.

The main results of this paper are (1) a general experimental protocol to measure out-of-time-order correlation functions and (2) a detailed cavity quantum electrodynamics proposal for implementing the protocol. We also briefly discuss the prospects for such measurements in systems of Rydberg atoms, trapped ions, and optical lattices.

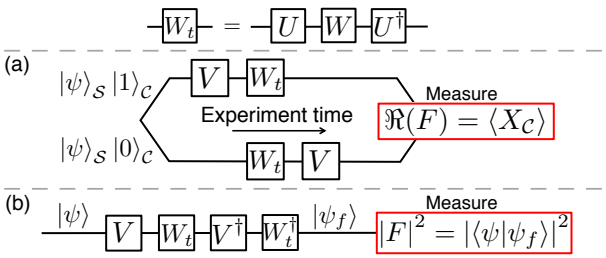

FIG. 1. Circuit diagrams of the interferometric and distinguishability protocols. (a) Given a control qubit $\mathcal{C}$, the interferometric protocol can measure F for the system $\mathcal{S}$ by applying different sequences of operators in the two interferometer arms. (b) Without a control qubit, the distinguishability protocol can measure $|F|^2$. The final measurement in both cases is indicated by a red box.

Physically, the out-of-time-order correlator F describes a gedankenexperiment in which we have the ability to reverse the flow of time. We compare two quantum states obtained by either (1) applying V, waiting for a time t, and then applying W; or (2) applying W at time t, going back in time to apply V at $t = 0$, and then letting time resume its forward progression again for time t [20, 21]. The correlator F measures the overlap between the two final states. In a many-body system where the time evolution is governed by a nontrivial interaction Hamiltonian, $F(t)$ diagnoses the spread of quantum information by measuring how quickly the interactions cause initially commuting operators V and W to fail to commute: $\langle|[W_t, V]|^2\rangle = 2(1 - \Re(F))$. Because F is always one in the absence of noncommutativity, it may be regarded as an intrinsically quantum mechanical variant of the Loschmidt echo [22], a paradigmatic probe of chaos.

The Loschmidt echo was measured in pioneering nuclear magnetism experiments [19], in many-body systems using "magic echo" and "polarization echo" techniques [23, 24], and in several other systems, e.g. [25] and the reviews [22, 26]. The Loschmidt echo can be related to the mean Lyapunov exponent of a corresponding chaotic classical system and to decoherence [27–29]. Out-of-time-order correlators can also be related to Lyapunov exponents [30] (reviewed in Supplementary Material) but typically explore longer time-scales than the Loschmidt echo.

As with the Loschmidt echo, the key experimental technology required is the ability to reverse the sign of the Hamiltonian. Recent progress in quantum engineering makes it conceivable that time can be reversed in complex quantum many-body systems. The other key technology needed to obtain full information about $F(t) = \langle W_t^\dagger V^\dagger W_t V\rangle$ is a certain type of many-body interferometry. A control qubit can be used to produce two branches in the many-body state [31–33]; measurement of the control qubit then provides direct access to the correlation function F (Fig. 1A). Even without the control qubit, an alternative protocol shown in Figure 1B allows us to measure the magnitude of F, which quantifies the indistinguishability of two states obtained by applying V and W_t in differing order.

Perfect control of the effective flow of time is not possible in the actual experiment, so we also discuss the impact of dissipation in the cavity model. Our time reversal protocol is the experimentally reasonable one: the Hamiltonian dynamics is reversed but the dissipative processes are not. It is thus important to establish that observables obtained from this partial time reversal protocol access the same physics as the analogous observables in the unitary protocol. We show that such a regime is achievable with state of the art cavities.

General protocol. Consider a quantum system $\mathcal{S}$ initialized in state $|\psi\rangle_{\mathcal{S}}$ and a control qubit $\mathcal{C}$ initialized in state $\frac{|0\rangle_{\mathcal{C}}+|1\rangle_{\mathcal{C}}}{\sqrt{2}}$. Let V and W be two unitary operators acting just on the system (not the control qubit), let $U(t) = e^{-iHt}$ denote time evolution of the system, and let $W_t = U(-t)WU(t)$ denote the Heisenberg operator at time t. The goal is to measure the four point function

$$F(t) = \langle W_t^\dagger V^\dagger W_t V\rangle. \tag{1}$$

For F to be interesting H must be a many-body Hamiltonian which contains interactions between different degrees of freedom. V and W may be taken to be simple operators which initially commute; in this case the physical picture is that the Heisenberg operator W_t grows in complexity as t increases and eventually fails to commute with V.

The *interferometric protocol* consists of two stages. First apply the gate sequence (illustrated in Figure 1A)

1. $I_{\mathcal{S}} \otimes |0\rangle\langle 0|_{\mathcal{C}} + V_{\mathcal{S}} \otimes |1\rangle\langle 1|_{\mathcal{C}}$ (control V)
2. $U(t)_{\mathcal{S}} \otimes I_{\mathcal{C}}$ (time evolution)
3. $W_{\mathcal{S}} \otimes I_{\mathcal{C}}$
4. $U(-t)_{\mathcal{S}} \otimes I_{\mathcal{C}}$ (backwards time evolution)
5. $V_{\mathcal{S}} \otimes |0\rangle\langle 0|_{\mathcal{C}} + I_{\mathcal{S}} \otimes |1\rangle\langle 1|_{\mathcal{C}}$

to prepare the state

$$\frac{(VW_t|\psi\rangle_{\mathcal{S}})|0\rangle_{\mathcal{C}} + (W_t V|\psi\rangle_{\mathcal{S}})|1\rangle_{\mathcal{C}}}{\sqrt{2}}. \tag{2}$$

Then measure the control qubit in the $|0\rangle \pm |1\rangle$ basis. The probability to obtain $|0\rangle \pm |1\rangle$ is

$$P(|0\rangle \pm |1\rangle) = \frac{1 \pm \Re\langle V^\dagger W_t^\dagger V W_t\rangle}{2} = \frac{1 \pm \Re(F)}{2}. \tag{3}$$

Thus

$$\langle X_{\mathcal{C}}\rangle = \Re(F) \tag{4}$$

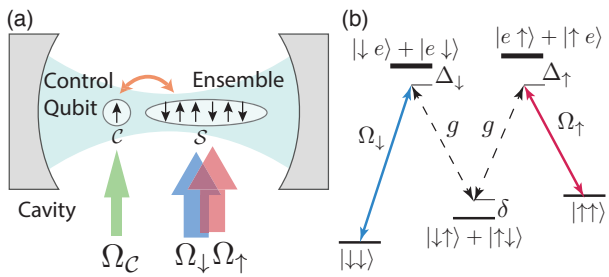

FIG. 2. Experimental scheme for measuring out-of-time-order correlators. (a) Atomic ensemble $\mathcal{S}$ and control qubit $\mathcal{C}$ in the waist of an optical cavity are driven from the side by control fields $\Omega_{\mathcal{C}}, \Omega_\uparrow, \Omega_\downarrow$. (b) Control fields $\Omega_{\uparrow,\downarrow}$ and cavity coupling g mediate 4-photon Raman transitions $|\downarrow\downarrow\rangle \leftrightarrow |\uparrow\uparrow\rangle$ in the atomic ensemble.

as desired. To obtain the imaginary part of F it suffices to measure $Y_{\mathcal{C}}$, $\langle Y_{\mathcal{C}}\rangle = \Im(F)$.

If the control qubit is not available then it is still possible to measure the magnitude of F using the *distinguishability protocol*. Initialize the system into state $|\psi\rangle$. Apply the gate sequence V, $U(t)$, W, $U(-t)$, $V^\dagger$, $U(t)$, $W^\dagger$, $U(-t)$ to prepare the state

$$|\psi_f\rangle = W_t^\dagger V^\dagger W_t V |\psi\rangle . \tag{5}$$

Finally, measure the projector $\Pi = |\psi\rangle\langle\psi|$; the result is $\langle\psi_f|\Pi|\psi_f\rangle = |F|^2$. $|F|^2$ is a measure of the distinguishability of the two branches and is expected to contain roughly the same timescales as F. In contrast to the interferometric protocol, the distinguishability protocol requires a careful choice of the initial state ψ, as the projection Π onto an arbitrary many-body state is generically challenging to implement.

Cavity QED proposal. As a quantum many-body system amenable to probing the out-of-time-order correlator, we consider a collection of two-level atoms (spins) that interact via their mutual coupling to one or more modes of an optical cavity. The setup is shown in Fig. 2. A drive laser incident from the side of the cavity generates interactions among all pairs of atoms it addresses. The sign of the interaction Hamiltonian H is set by the laser frequency, making the magnitudes of out-of-time correlators experimentally accessible via the distinguishability protocol. To enable measurements of the phase of the out-of-time correlator via many-body interferometry, a single individually addressable atom can serve as a control qubit. The qubit state can be mapped onto the presence or absence of a photon in the cavity, which in turn influences the entire ensemble [31].

The cavity-mediated interactions within the ensemble generically take the form of a nonlocal spin model [34–36]

$$H = \sum_{ij} J_{ij} s_i^x s_j^x + h.c., \tag{6}$$

where $\mathbf{s}_i$ is a pseudo-spin operator representing two internal atomic states (e.g., hyperfine states) $|s_i^z = \pm 1/2\rangle$. For N atoms at positions r_i with couplings $g_\alpha(r_i)$ to a set of degenerate cavity modes indexed by α, the spin-spin couplings are given by

$$J_{ij} = \sum_\alpha \frac{\Omega_\uparrow^*(r_i)\Omega_\downarrow(r_j)}{\Delta_\uparrow\Delta_\downarrow}\frac{g_\alpha(r_i)g_\alpha^*(r_j)}{\delta}, \tag{7}$$

where $\Omega_{\uparrow,\downarrow}$ are the Rabi frequencies of the drive fields, detuned by $\Delta_{\uparrow,\downarrow}$ from atomic resonance, and δ is the detuning of the two-photon transition mediated by the drive fields and cavity couplings g_α.

The key features of this system are that the sign of the interaction is controllable via the two-photon detuning δ [37], that the interaction can be switched off by turning off the drive fields, and that the full graph of interactions depends both on the atomic positions and on the spatial structure of the cavity modes and control fields. Furthermore, it is possible to produce noncommuting s^+s^- type interactions, to add fields in any direction, and to include time dependence in the Hamiltonian. This versatility provides opportunities for studying a range of many-body phenomena, from quantum glasses [35, 36, 38] to random circuit models that mimic the fast scrambling dynamics of black holes [39].

A natural out-of-time-order correlator to measure is one where the operations V and W involve independent rotations of the spins. The control qubit in Fig. 2 provides a straightforward means of measuring such a correlator [31]. Temporarily turning off the interaction Eq. 6 and converting the control qubit state $|n\rangle_{\mathcal{C}}$ (with $n \in \{0,1\}$) into an n-photon state of the cavity produces a differential a.c. Stark shift $\propto n$ between each of the ensemble atoms' two levels. The result is a collective controlled phase gate

$$Z_\phi^{\mathcal{C}} = I_{\mathcal{S}} \otimes |0\rangle\langle 0|_{\mathcal{C}} + e^{-i\phi S_z^{\mathcal{S}}} \otimes |1\rangle\langle 1|_{\mathcal{C}} , \tag{8}$$

where $S_z^{\mathcal{S}} = \sum_i s_i^z$. This gate can directly serve as the controlled-V step in the interferometer of Fig. 1A, with $V = e^{-i\phi S_z^{\mathcal{S}}}$, or can readily be transformed into a controlled rotation about any axis. The operation W can simply be a global spin rotation applied irrespective of the control qubit state. In particular, W_t is applied by sandwiching the rotation W between evolutions under $+H$ and $-H$ (Fig. 1), generated by illuminating the ensemble $\mathcal{S}$ with control fields of two-photon detuning $\pm\delta$.

For purposes of illustration, we calculate F for a globally interacting spin model obtained by coupling all atoms uniformly to a single cavity mode. Here, the Hamiltonian of Eq. 6 reduces to a "one-axis twisting" Hamiltonian $H_{\text{twist}} = \chi S_x^2$, where $\mathbf{S} = \sum_i \mathbf{s}_i$ and the total spin is $S = N/2$. Fig. 3 shows a plot of F for an initial state $|\hat{y}\rangle = |S_y = S\rangle$ and rotations $V = W = e^{-i\phi S_z}$ with $\phi = \pi/4$. As we discuss below, such a large controlled rotation angle is neither necessary nor sustainable at higher

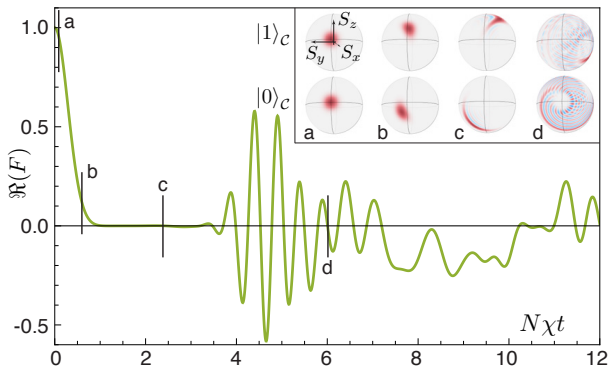

FIG. 3. Interferometric protocol for unitary S_x^2 dynamics at $N = 50$. For an initial coherent state $|\hat{y}\rangle$ and rotation angle $\phi = \pi/4$, $\Re(F)$ (green) exhibits decay at short times (a,b), a period of quiescence (c), and subsequent oscillations (d). Inset: States of the two interferometer arms at various times. Illustrated is the Wigner quasiprobability distribution of the collective spin for $N = 50$ atoms.

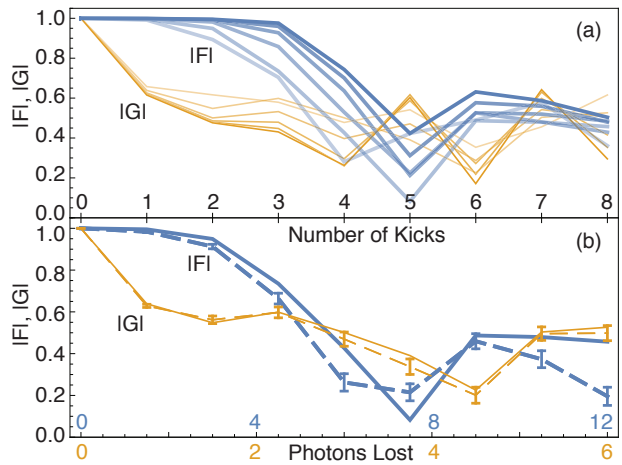

FIG. 4. Interferometric protocol for the kicked top model. (a) Unitary time-ordered correlators $|G(t)|$ (thin yellow) and out-of-time-order correlators $|F(t)|$ (thick blue) for various atom numbers $N = 50, 100, 200, 300, 400, 500$, kick strength $k = 3$, rotation angle $\phi = 1/\sqrt{N}$, and initial coherent spin state $e^{-iS_y\pi/4}e^{-iS_z\pi/4}|\hat{x}\rangle$. (b) Time-ordered correlator $|G(t)|$ (thin yellow) and out-of-time-order correlator $|F(t)|$ (thick blue) for $N = 100$. Solid lines show unitary evolution, dashed lines with statistical error bars show dissipative evolution at cooperativity $\eta = 100$ and detuning $\delta = 10\kappa$, with 200 quantum trajectories per point. Horizontal axes show kick number (black) and mean number of photons lost via decay processes during the measurement of the time-ordered (yellow) and out-of-time-order (blue) correlators (see Supplementary Material).

atom numbers, but it serves to illustrate in exaggerated form the processes leading to the decay of F.

The Bloch spheres in Fig. 3 show the Wigner quasiprobability distributions [40] for the two arms of the interferometer at various times in the evolution. The two arms begin in the same state at $t = 0$ but rapidly diverge to opposite sides of the sphere. During this time, the evolution is consistent with the classical motion of a spin coherent state. By the time the two arms of the interferometer reach antipodes on the Bloch sphere, the Wigner distributions have started to spread substantially. These numerical results lead to a picture of F in which the initial decay corresponds to the divergence of classical trajectories while the later fluctuations correspond to the spread of the quantum state over the entire Hilbert space. However, the S_x^2 Hamiltonian is not a chaotic model, so it can only partially illuminate the physics of F.

The S_x^2 Hamiltonian may be modified to produce a chaotic system by periodically applying a rapid S_z rotation to the system—i.e. a "kick." This kicked top model has been studied both theoretically and experimentally [41–43]. The stroboscopic dynamics are described by repeated application of the unitary operator U associated with each kick,

$$U = e^{-i\frac{k}{2S}S_x^2}e^{-ipS_z}, \tag{9}$$

where k measures the strength of interactions and p measures the size of the rotational kick. Following Haake et al. [41], it is convenient to set $p = \pi/2$; then the corresponding classical model describes motion on the Bloch sphere which is mostly regular for small k and mostly chaotic for large k. The semi-classical limit is the limit of large S, whereas previous experimental work has studied the case $S = 3$ [42]. The cavity-QED implementation proposed here, where the spin is scalable from the small-S quantum regime to the semi-classical limit, provides an ideal testbed for probing the physics of the out-of-time correlator in a paradigmatic chaotic system.

We compare the out-of-time correlator $F(t)$ with a time-ordered correlator $G(t) = \langle V_t^\dagger V\rangle$, similar to a Loschmidt echo, for the kicked top at a variety of atom numbers $N = 2S$ in Fig. 4. We take V and W to be S_z rotations by a small angle $\phi = 1/\sqrt{2S}$. This scaling of ϕ with S is chosen so that W and V represent simple operators for which we expect to observe a separation of timescales between time-ordered and out-of-time-order correlators as $S \to \infty$ (see Supplementary Material). We plot both correlators for an initial coherent state $e^{-iS_y\pi/4}e^{-iS_z\pi/4}|S_x = S\rangle$ and kick strength $k = 3$, first assuming unitary dynamics. Even at finite N, the out-of-time-order correlator (blue) decays on a significantly longer timescale than the time-ordered correlator (yellow). While the decay time for the time-ordered correlator is roughly independent of N, the decay time for the out-of-time-order correlator grows with N. A preliminary analysis is consistent with this growth being logarithmic in N.

In a realistic implementation, the measurement of F can be compromised by two forms of dissipation: leakage of photons from the cavity of linewidth κ; and decay

from the atomic excited state of linewidth Γ. The attainable fidelities of the controlled phase gate and of the time-reversed Hamiltonian thus both depend on the cooperativity $\eta = 4g^2/\kappa\Gamma$, where $2g$ is the vacuum Rabi frequency. For an ensemble of N atoms, the maximum achievable controlled phase rotation is of order $\sqrt{\eta/N}$, while observing the onset of chaos in the quantum kicked top requires $\eta > (k \ln N)^2$ (see Supplementary Material). Thus, dissipation can be kept small at modest atom number $N \lesssim 10^2$ in a state-of-the-art strong coupling cavity with $\eta \sim 10^1 - 10^2$ [44, 45], but it cannot be entirely neglected.

To verify that a realistic non-unitary evolution suffices to estimate the out-of-time correlator, we simulate measurements of F and G in the kicked-top model using quantum trajectories (see Supplementary Material). The results of the full dissipative evolution for the interferometric protocol are plotted in Fig. 4(b) for a cavity cooperativity $\eta = 100$ (dashed lines) and compared with the unitary case (solid lines). Although dissipation eventually degrades the signal, the early-time dissipative evolution is faithful to the unitary evolution and the difference in timescales between F and G can be easily resolved.

Discussion. In the near term, the above measurements can be carried out in the single-mode cavity setting, where the classically chaotic kicked-top model presents an opportunity to study out-of-time-order correlators in great detail. The protocol can be translated directly to trapped-ion experiments by replacing photon-mediated with phonon-mediated interactions [46, 47], which enable simulations of transverse-field Ising models with a tunable interaction range [2, 3, 48]. Neutral Rydberg atoms likewise offer possibilities both for implementing a qubit-controlled rotation [33] and for engineering spatially local spin models [49, 50] with either sign of interaction.

Reversing time is also possible in optical-lattice implementations of Hubbard models, where the Hamiltonian consists of an interaction term and a hopping term. Feshbach resonances can be used to control the magnitude and sign of the interaction, while the sign of the hopping term can be controlled by modulating the lattice potential [51–53]. A qubit-controlled phase shift can be imprinted locally using either an impurity atom [54, 55] or a control atom specified by high-resolution addressing [32] in a quantum gas microscope [56, 57]. Even without the control qubit, the distinguishability protocol can be applied. For special initial states—including superfluids or Mott insulators in two dimensions—it can be performed by established techniques of time-of-flight or *in situ* imaging.

Imperfect reversal of H, coupling to an environment, and imperfect measurements all degrade the signal of interest. For the kicked top model we showed that early time physics of the out-of-time-order correlator can already be observed with state of the art cavities. Another natural objective would be to determine whether the onset of large fluctuations observed in Fig. 3 coincides with either the Ehrenfest or Liouville break times, corresponding to divergence of the quantum mechanical prediction from the evolution of classical trajectories or phase space distributions, respectively [27, 58]. More generally we expect that much can be learned about chaos and decoherence in quantum many-body systems from the imperfect experimental models.

We conclude with a few comments about the problem of black hole simulation and detection. A black hole is a thermal system, so to mimic the physics of scrambling in black hole states it must be possible to prepare thermal states. This can be accomplished by appealing to closed system thermalization [59–61]. One would initialize the system into a suitable pure state, evolve the system for an equilibration time, and then execute the out-of-time-order protocol. Thermalization in closed systems is an interesting topic in its own right, e.g. [62], and out-of-time-order correlators offer senstive probes of thermalization (or the lack thereof). For example, they can distinguish single-particle localized [63], many-body localized [64], and ergodic phases as will be reported elsewhere.

Just constructing a model system which has the scrambling properties of a black hole is a highly nontrivial task. A direct route is to attempt to realize a matrix model or gauge theory in a quantum simulator, but this is currently a remote prospect. Recently, Kitaev has shown that a model consisting of random four fermion interactions has black hole-like out-of-time-order correlations [65]. In fact, this model is a close relative of a class of random non-local spin models proposed to study quantum spin glasses [38]. Such a random spin model consists of interactions like the ones in Eq. 6, so another route to simulating black holes is to pursue quantum scrambling in multi-mode cavities. Finding a paramagnetic state that scrambles is not trivial, but adding a periodic external perturbation as in the kicked top should aid in melting any glass order.

Finally, then, the out-of-time-order protocol presented here, when combined with the fact that black holes saturate the chaos bound [6, 10], suggests a sharp experimental test for the presence of a black hole. One would use the out-of-time-order protocol to extract a Lyapunov exponent from measurements of the early time growth of $F(t)$. If the exponent saturates the chaos bound then the conjecture is that the dual state contains a black hole. One advantage of this test is that it focuses on the universal Lyapunov exponent and not on the details of the equilibrium state or of time-ordered correlators.

M.S.-S. and G. B. acknowledge support from the NSF, the AFOSR, and the Alfred P. Sloan Foundation. P. H. and B. S. appreciate support from the Simons Foundation and CIFAR. We thank S. Shenker, N. Yao, and E. Demler for enlightening discussions.

* bswingle@stanford.edu

[1] M. Cheneau, P. Barmettler, D. Poletti, M. Endres, P. Schauß, T. Fukuhara, C. Gross, I. Bloch, C. Kollath, and S. Kuhr, Nature **481**, 484 (2012).
[2] P. Richerme, Z.-X. Gong, A. Lee, C. Senko, J. Smith, M. Foss-Feig, S. Michalakis, A. V. Gorshkov, and C. Monroe, Nature **511**, 198 (2014).
[3] P. Jurcevic, B. P. Lanyon, P. Hauke, C. Hempel, P. Zoller, R. Blatt, and C. F. Roos, Nature **511**, 202 (2014).
[4] J. Eisert, M. Friesdorf, and C. Gogolin, Nat Phys **11**, 124 (2015).
[5] E. Lieb and D. Robinson, Communications in Mathematical Physics **28**, 251 (1972).
[6] S. H. Shenker and D. Stanford, Journal of High Energy Physics **3**, 67 (2014), arXiv:1306.0622 [hep-th].
[7] J. D. Bekenstein, Phys. Rev. **D7**, 2333 (1973).
[8] P. Hayden and J. Preskill, Journal of High Energy Physics **9**, 120 (2007), arXiv:0708.4025 [hep-th].
[9] Y. Sekino and L. Susskind, Journal of High Energy Physics **10**, 065 (2008), arXiv:0808.2096 [hep-th].
[10] J. Maldacena, S. H. Shenker, and D. Stanford, ArXiv e-prints (2015), arXiv:1503.01409 [hep-th].
[11] G. Hooft, arXiv preprint gr-qc/9310026 (1993).
[12] L. Susskind, Journal of Mathematical Physics **36**, 6377 (1995).
[13] J. Maldacena, International Journal of Theoretical Physics **38**, 1113 (1999), hep-th/9711200.
[14] T. Banks, W. Fischler, S. H. Shenker, and L. Susskind, Phys. Rev. D **55**, 5112 (1997), hep-th/9610043.
[15] O. Aharony, S. S. Gubser, J. Maldacena, H. Ooguri, and Y. Oz, Phys. Rep. **323**, 183 (2000), hep-th/9905111.
[16] E. Zohar, J. I. Cirac, and B. Reznik, Reports on Progress in Physics **79**, 014401 (2016), arXiv:1503.02312 [quant-ph].
[17] S. W. Hawking, Nature **248**, 30 (1974).
[18] A. Kitaev, talk at Fundamental Physics Prize Symposium Nov. 10, 2014 (2014).
[19] E. L. Hahn, Phys. Rev. **80**, 580 (1950).
[20] S. H. Shenker and D. Stanford, Journal of High Energy Physics **2014**, 1 (2014).
[21] D. A. Roberts, D. Stanford, and L. Susskind, Journal of High Energy Physics **2015**, 1 (2015).
[22] A. Goussev, R. A. Jalabert, H. M. Pastawski, and D. Wisniacki, ArXiv e-prints (2012), arXiv:1206.6348 [nlin.CD].
[23] W.-K. Rhim, A. Pines, and J. S. Waugh, Phys. Rev. B **3**, 684 (1971).
[24] S. Zhang, B. H. Meier, and R. R. Ernst, Phys. Rev. Lett. **69**, 2149 (1992).
[25] M. F. Andersen, A. Kaplan, and N. Davidson, Phys. Rev. Lett. **90**, 023001 (2003).
[26] T. Gorin, T. Prosen, T. H. Seligman, and M. Žnidarič, Physics Reports **435**, 33 (2006).
[27] W. H. Zurek and J. P. Paz, Phys. Rev. Lett. **72**, 2508 (1994).
[28] R. A. Jalabert and H. M. Pastawski, Phys. Rev. Lett. **86**, 2490 (2001).
[29] F. M. Cucchietti, D. A. R. Dalvit, J. P. Paz, and W. H. Zurek, Phys. Rev. Lett. **91**, 210403 (2003).
[30] A. I. Larkin and Y. N. Ovchinnikov, Soviet Journal of Experimental and Theoretical Physics **28**, 1200 (1969).
[31] L. Jiang, G. K. Brennen, A. V. Gorshkov, K. Hammerer, M. Hafezi, E. Demler, M. D. Lukin, and P. Zoller, Nature Physics **4**, 482 (2008), arXiv:0711.1365 [quant-ph].
[32] D. A. Abanin and E. Demler, Physical review letters **109**, 020504 (2012).
[33] M. Müller, I. Lesanovsky, H. Weimer, H. P. Büchler, and P. Zoller, Phys. Rev. Lett. **102**, 170502 (2009).
[34] A. S. Sørensen and K. Mølmer, Physical Review A **66**, 022314 (2002).
[35] S. Gopalakrishnan, B. L. Lev, and P. M. Goldbart, Phys. Rev. Lett. **107**, 277201 (2011).
[36] P. Strack and S. Sachdev, Physical Review Letters **107**, 277202 (2011), arXiv:1109.2119 [cond-mat.quant-gas].
[37] E. Davis, G. Bentsen, and M. Schleier-Smith, Phys. Rev. Lett. **116**, 053601 (2016).
[38] S. Sachdev and J. Ye, Phys. Rev. Lett. **70**, 3339 (1993).
[39] N. Lashkari, D. Stanford, M. Hastings, T. Osborne, and P. Hayden, Journal of High Energy Physics **2013**, 1 (2013).
[40] J. P. Dowling, G. S. Agarwal, and W. P. Schleich, Phys. Rev. A **49**, 4101 (1994).
[41] F. Haake, M. Kuś, and R. Scharf, Zeitschrift für Physik B Condensed Matter **65**, 381 (1987).
[42] S. Chaudhury, A. Smith, B. E. Anderson, S. Ghose, and P. S. Jessen, Nature (London) **461**, 768 (2009).
[43] X. Wang, S. Ghose, B. C. Sanders, and B. Hu, Phys. Rev. E **70**, 016217 (2004), quant-ph/0312047.
[44] Y. Colombe, T. Steinmetz, G. Dubois, F. Linke, D. Hunger, and J. Reichel, Nature **450**, 272 (2007).
[45] J. Klinder, H. Keßler, M. R. Bakhtiari, M. Thorwart, and A. Hemmerich, Phys. Rev. Lett. **115**, 230403 (2015).
[46] J. I. Cirac and P. Zoller, Phys. Rev. Lett. **74**, 4091 (1995).
[47] K. Mølmer and A. Sørensen, Physical Review Letters **82**, 1835 (1999).
[48] J. G. Bohnet, B. C. Sawyer, J. W. Britton, M. L. Wall, A. M. Rey, M. Foss-Feig, and J. J. Bollinger, arXiv preprint arXiv:1512.03756 (2015).
[49] R. van Bijnen and T. Pohl, Phys. Rev. Lett. **114**, 243002 (2015).
[50] A. W. Glaetzle, M. Dalmonte, R. Nath, C. Gross, I. Bloch, and P. Zoller, Phys. Rev. Lett. **114**, 173002 (2015).
[51] J. Struck, C. Ölschläger, M. Weinberg, P. Hauke, J. Simonet, A. Eckardt, M. Lewenstein, K. Sengstock, and P. Windpassinger, Phys. Rev. Lett. **108**, 225304 (2012).
[52] J. Struck, C. lschlger, R. Le Targat, P. Soltan-Panahi, A. Eckardt, M. Lewenstein, P. Windpassinger, and K. Sengstock, Science **333**, 996 (2011), http://www.sciencemag.org/content/333/6045/996.full.pdf.
[53] M. Aidelsburger, M. Atala, S. Nascimbène, S. Trotzky, Y.-A. Chen, and I. Bloch, Phys. Rev. Lett. **107**, 255301 (2011).
[54] M. Knap, A. Shashi, Y. Nishida, A. Imambekov, D. A. Abanin, and E. Demler, Physical Review X **2**, 041020 (2012).
[55] M. Cetina, M. Jag, R. S. Lous, J. T. M. Walraven, R. Grimm, R. S. Christensen, and G. M. Bruun, Phys. Rev. Lett. **115**, 135302 (2015).
[56] W. S. Bakr, J. I. Gillen, A. Peng, S. Fölling, and M. Greiner, Nature **462**, 74 (2009).
[57] C. Weitenberg, M. Endres, J. F. Sherson, M. Cheneau, P. Schauss, T. Fukuhara, I. Bloch, and S. Kuhr, Nature **471**, 319 (2011).

[58] L. Ballentine, Y. Yang, and J. Zibin, Physical review A **50**, 2854 (1994).
[59] M. Srednicki, Phys. Rev. E **50**, 888 (1994), cond-mat/9403051.
[60] J. M. Deutsch, Phys. Rev. A **43**, 2046 (1991).
[61] N. Linden, S. Popescu, A. J. Short, and A. Winter, Phys. Rev. E **79**, 061103 (2009), arXiv:0812.2385 [quant-ph].
[62] T. Langen, S. Erne, R. Geiger, B. Rauer, T. Schweigler, M. Kuhnert, W. Rohringer, I. E. Mazets, T. Gasenzer, and J. Schmiedmayer, Science **348**, 207 (2015), http://www.sciencemag.org/content/348/6231/207.full.pdf.
[63] P. W. Anderson, Phys. Rev. **109**, 1492 (1958).
[64] D. M. Basko, I. L. Aleiner, and B. L. Altshuler, Annals of Physics **321**, 1126 (2006), cond-mat/0506617.
[65] A. Kitaev, talk at KITP Santa Barbara (2015).
[66] R. A. Jalabert and H. M. Pastawski, Physical review letters **86**, 2490 (2001).
[67] P. Jacquod, P. G. Silvestrov, and C. W. Beenakker, Physical Review E **64**, 055203 (2001).
[68] H. Quan, Z. Song, X. Liu, P. Zanardi, and C. Sun, Physical review letters **96**, 140604 (2006).
[69] J. Liu, W. Wang, C. Zhang, Q. Niu, and B. Li, Physical Review A **72**, 063623 (2005).
[70] P. R. Levstein, G. Usaj, and H. M. Pastawski, The Journal of chemical physics **108**, 2718 (1998).
[71] J. Maldacena, Journal of High Energy Physics **4**, 021 (2003), hep-th/0106112.
[72] S. H. Shenker and D. Stanford, Journal of High Energy Physics **5**, 132 (2015), arXiv:1412.6087 [hep-th].
[73] A. J. Daley, Adv. Phys. **63**, 77 (2014), arXiv:1405.6694 [quant-ph].
[74] L. Jiang, G. K. Brennen, A. V. Gorshkov, K. Hammerer, M. Hafezi, E. Demler, M. D. Lukin, and P. Zoller, Nat Phys **4** (2008), 10.1038/nphys943.
[75] M. H. Schleier-Smith, I. D. Leroux, and V. Vuletić, Phys. Rev. A **81**, 021804 (2010).

Measuring time-ordered correlation functions

Here we demonstrate that time-ordered correlation functions can be measured using only forward time evolution.

Suppose we want to measure a correlation function of the form

$$G(t,s) = \left\langle (V_n(t_n)...V_1(t_1))^\dagger (W_n(s_n)...W_1(s_1)) \right\rangle \quad (10)$$

where V_i and W_j are unitary operators (which may or may not all be distinct) acting on some system A and $\{t_i\}$ and $\{s_i\}$ are nondecreasing time sequences. First, observe that G is a time ordered correlation function. All the W and V operators are manifestly in time order within their respective parenthesis and the $\dagger$ on the V operators reverses the order of all such operators. Hence the time labels of the operators in G first increase (s part) and then decrease (t part).

Note that by choosing some of the V_i or W_j to be identity operators we may assume without loss of generality that $\{s_i\}$ and $\{t_j\}$ have the same number of points and that $t_i = s_i$. Then we proceed as in the general protocol above by introducing a control qubit $\mathcal{C}$ and initializing the total system into the state

$$|\text{initial}\rangle = |\psi\rangle_A \frac{|0\rangle_\mathcal{C} + |1\rangle_\mathcal{C}}{\sqrt{2}}. \quad (11)$$

Then apply the gate sequence

1. $e_\mathcal{S}^{-it_1 H} \otimes I_\mathcal{C}$
2. $(W_1)_\mathcal{S} \otimes |0\rangle\langle 0|_\mathcal{C} + (V_1)_\mathcal{S} \otimes |1\rangle\langle 1|_\mathcal{C}$
3. $e_\mathcal{S}^{-i(t_2-t_1)H} \otimes I_\mathcal{C}$
4. $(W_2)_\mathcal{S} \otimes |0\rangle\langle 0|_\mathcal{C} + (V_2)_\mathcal{S} \otimes |1\rangle\langle 1|_\mathcal{C}$

j. ...

2n-1. $e_\mathcal{S}^{-i(t_n-t_{n-1})H} \otimes I_\mathcal{C}$

2n. $(W_n)_\mathcal{S} \otimes |0\rangle\langle 0|_\mathcal{C} + (V_n)_\mathcal{S} \otimes |1\rangle\langle 1|_\mathcal{C}$

to produce the final state

$$|\text{final}\rangle = \frac{(e^{-it_n H} W_n(t_n)...W_1(t_1)|\psi\rangle)_\mathcal{S}|0\rangle_\mathcal{C}}{\sqrt{2}} + \frac{(e^{-it_n H} V_n(t_n)...V_1(t_1)|\psi\rangle)_\mathcal{S}|1\rangle_\mathcal{C}}{\sqrt{2}}. \quad (12)$$

Some comments are in order. The time evolution prefactor common to both interference paths occurs because in the above gate protocol we did not actually apply $W_n(t_n) = e^{it_n H} W_n e^{-it_n H}$ but rather just $W_n e^{-it_n H}$, so this operator prefactor cancels the reverse time evolution in the definition of $W_n(t_n)$ and $V_n(t_n)$. However, because it is common to both interference paths it has no effect on the interferometer and we may as well work with $W_n(t_n)$ and $V_n(t_n)$ as indicated. Furthermore, despite the formal appearance of factors of $U(-t_i)$ in the definition of the various $V_i(t_i)$, etc., no backwards time evolution is ever performed. The forward time evolution involved in defining $V_{k+1}(t_{k+1})$ always cancels the backwards time evolution in $V_k(t_k)$ so that only net forward evolution is required.

The final result is

$$\langle \text{final}|X_\mathcal{C}|\text{final}\rangle = \Re(G). \quad (13)$$

This justifies the claims that time ordered correlation functions can always be measured without reversing time. Of course, this is not to imply that the above interferometric protocol is the best way to measure G; all we claim is that the measurement is possible without reversing time.

Out-of-time-order correlators of Hermitian operators

If we are interested in Hermitian operators instead of unitary operators, there is a more complicated general protocol. The idea is to consider unitaries perturbed from the identity by the hermitian operator of interest (times a small coefficient). By coupling in additional marker or flag qubits which are flipped when the hermitian operator acts on the system and post selecting on measurements where the marker qubit has been flipped we can access to states where the hermitian operator has been applied. In brief, if $V_{A\,\text{flag}} = e^{i\epsilon O_A \otimes X_{\text{flag}}}$ then $V_{\mathcal{S}\,\text{flag}} |\psi\rangle_{\mathcal{S}} |0\rangle_{\text{flag}} \approx |\psi\rangle_{\mathcal{S}} |0\rangle_{\text{flag}} + i\epsilon O_{\mathcal{S}} |\psi\rangle_{\mathcal{S}} |1\rangle_{\text{flag}}$ and post selecting on the flag $= 1$ produces a state proportional to $O_{\mathcal{S}} |\psi\rangle_{\mathcal{S}}$. Of course, this is again not necessarily a very efficient way of making the measurement.

As an example, take the interferometric protocol above and introduce three additional flag qubits. The unitaries W and V are taken to be of the form $e^{i\epsilon O_{\mathcal{S}}^{W,V} \otimes X_{\text{flag}}}$ and the three flag qubits are used to check that (1) the first control V applies O^V, (2) the middle W applies O^W, and (3) the final control V applies O^V. Conditioned on all three flag qubits being equal to one, something which occurs with probability $\epsilon^3(\langle O_t^W O^V O^V O_t^W\rangle + \langle O^V O_t^W O_t^W O^V\rangle)/2$, we obtain the normalized state

$$\frac{O^V O_t^W |\psi\rangle_A |0\rangle_{\mathcal{C}} + O_t^W O^V |\psi\rangle |1\rangle_{\mathcal{C}}}{\sqrt{\langle O_t^W O^V O^V O_t^W\rangle + \langle O^V O_t^W O_t^W O^V\rangle}}. \tag{14}$$

Measurement of $X_{\mathcal{C}}$ in this state now yields

$$\langle X_{\mathcal{C}}\rangle = \frac{\langle O^V O_t^W O^V O_t^W\rangle + \langle O_t^W O^V O_t^W O^V\rangle}{\langle O_t^W O^V O^V O_t^W\rangle + \langle O^V O_t^W O_t^W O^V\rangle}; \tag{15}$$

this is the normalized version of $\Re(F)$ for hermitian operators. Note that the normalization consists only of time ordered correlation functions.

A review of chaos, out-of-time-order correlators, and black holes

Here we review the basic connection between out-of-time-order correlations and chaos first observed in [30]. We then briefly discuss the relationship between out-of-time-order correlators and Loschmidt echoes. Finally, we quickly recall some basics of chaos in black hole systems that further clarify the timescales discussed in the main text.

Consider a single particle with position q and momentum p and let $q_t(q_0, p_0)$ and $p_t(q_0, p_0)$ denote the trajectories as a function of time t with initial conditions (q_0, p_0). If the motion is chaotic, then we expect sensitive dependence on initial conditions,

$$\frac{\partial q_t}{\partial q_0} \sim e^{\lambda t} \tag{16}$$

with λ a Lyapunov exponent. The derivative of q_t with respect to the initial condition is most naturally written as a Poisson bracket,

$$\frac{\partial q_t}{\partial q_0} = \{q_t, p_0\}_P, \tag{17}$$

where the Poisson bracket is defined as

$$\{A, B\}_P = \frac{\partial A}{\partial q_0}\frac{\partial B}{\partial p_0} - \frac{\partial A}{\partial p_0}\frac{\partial B}{\partial q_0}. \tag{18}$$

Quantum mechanically the Poisson bracket becomes the commutator of q_t and p_0, and the correspondence principle gives

$$[q_t, p_0] \sim i\hbar\{q_t, p_0\}_P \sim i\hbar e^{\lambda t}. \tag{19}$$

This quantity can be accessed elegantly using unitary operators (we set $q_0, p_0 \to q, p$ for notational simplicity). Let $W = e^{iaq}$ and $V = e^{ibp}$ and consider the multiplicative commutator $W_t^\dagger V^\dagger W_t V$. In the limit of small a and b and short time t the multiplicative commutator reduces to the exponential of the usual commutator,

$$W_t^\dagger V^\dagger W_t V \approx e^{i^2 ab[q_t, p]} \approx e^{-iab\hbar e^{\lambda t}}. \tag{20}$$

The parameters entering this equation will depend on the state of the system as well, so a more general statement is

$$\langle W_t^\dagger V^\dagger W_t V\rangle \sim e^{-iab\hbar e^{\lambda t}}. \tag{21}$$

Hence the phase of this correlation function initially diverges rapidly with t and, as higher order terms become important, the magnitude will also begin to decay. To the best of our knowledge, such out-of-time-order correlators were first discussed in the context of superconductivity in [30].

What is the physical meaning of this correlation function? It directly measures the overlap between two states,

$$e^{iHt} W e^{-iHt} V |\psi_0\rangle \tag{22}$$

and

$$V e^{iHt} W e^{-iHt} |\psi_0\rangle, \tag{23}$$

and hence physically represents the sensitivity of the system to applying V then W_t versus applying W_t then V. Thus it measures sensitivity to initial conditions or the "butterfly effect". Furthermore, the key role played by reversing time, that is evolving with e^{iHt} as well as with e^{-iHt}, should be apparent.

Supposing that the dimensionless quantity $ab\hbar = \epsilon$ is small ($1/ab$ represents a natural classical action scale in the problem), then the time required for F to develop a significant phase is $\lambda^{-1}\log\left(\frac{1}{\epsilon}\right)$, known as the Ehrenfest time. It is the time required for the wavepacket to spread

to a size of order the typical classical action. In a strongly interacting quantum system at finite temperature we expect $\lambda^{-1} \sim \tau = \frac{\hbar}{k_B T}$; in fact this a bound under the assumptions of [10]. Thus time-ordered correlation functions, which typically decay after a time of order λ^{-1}, can decay parametrically faster than out-of-time-order correlation functions since the scale $\lambda^{-1} \log\left(\frac{1}{\epsilon}\right)$ is much greater than λ^{-1} if ϵ is small.

In the kicked top model, the role of $\hbar$ is played by the inverse spin $1/S$. In the large S limit the rescaled operator $\mathbf{S}/S$ becomes classical with the unit sphere interpreted as a classical phase space; $1/S$ sets the natural unit of phase space volume so that the total number of states is of order S. The classical dynamics on the unit sphere is chaotic and there are two Lyapunov exponents, $\pm\lambda$, which depend on the location in space space. The analog of the Ehrenfest time is thus $\lambda^{-1} \log S$. Choosing V and W to be S_z rotations by angle ϕ, the scaling $\phi \sim 1/\sqrt{S}$ is designed so that at large S time-ordered correlations decay on the timescale λ^{-1} while out-of-time-order correlations decay on the longer timescale $\lambda^{-1} \log S$.

Chaos is also closely associated with the concept of the Loschmidt echo. The basic definition of the echo is

$$\mathcal{L}(t) = |\langle\psi|e^{iH't}e^{-iHt}|\psi\rangle|^2. \tag{24}$$

Going back to the work of Peres, this object probes the sensitivity of the system to a perturbation $\Delta H = H' - H$ in the dynamics. The echo has been studied extensively in single particle systems with a semiclassical limit, where it has been related to chaos in the corresponding classical model [66, 67]. While most work is done for single particle dynamics due to the relative ease of numerics, the echo has also been studied in some many-body systems including spin chains [68] and Bose-Einstein condensates [69]. Experimentally, work on this subject goes back to Hahn's spin echo technique [19]. Subsequently, a variety of experimental platforms have realized echo measurements with varying levels of isolation and control. In the context of NMR there have even been many-body echo measurements for special dipolar-interacting models starting with [70]. (See [22, 26] for reviews of theoretical and experimental work in the area.)

In fact there are multiple kinds of echo measurements. The global echo is $\mathcal{L}(t) = |\langle\psi|e^{iH't}e^{-iHt}|\psi\rangle|^2$, written above. Given two operators A and B a local echo, $\mathcal{L}_{loc}(t) = \langle\psi|e^{iH't}e^{-iHt}Ae^{iHt}e^{-iH't}B|\psi\rangle$, can also be defined. In the context of a magnetic system where A and B are spin operators, the local echo is related to revivals of the polarization after an echo sequence applied to a state with an initially polarized local spin. For example, if $|\psi\rangle$ were a state perturbed from local equilibrium by a local spin flip, then the local echo with $B = I$ and $A = S^z$ would correspond to the polarization after the echo sequence.

There are also multiple timescales which can enter echo measurements. When the corresponding classical dynamics is chaotic, the Lyapunov exponents λ, which govern the exponential divergence (or convergence) of nearby trajectories, define an important set of timescales. There is also a scattering time related related to how often the particle interacts with the potential (or with other particles). The quantum system is also characterized by its inverse level spacing, sometimes called the Heisenberg time. Finally, there is the so-called breaking time or Ehrenfest time which is the timescale after which the semiclassical approximation to the Wigner function breaks. In fact, one can define multiple breaking times associated with the breakdown of semiclassicality as measured by a variety of quantities.

Following the sketch above, the timescales of most direct relevance to the out-of-time-order correlator in a single-particle system are the inverse of the largest Lyapunov exponent and the Ehrenfest time. In particular, we saw that the out-of-time-order correlator could be expected to diverge from one at a rate controlled by a Lyapunov exponent and that it became small at times of order the Ehrenfest time. Conventional time-ordered correlation functions would be expected to decay on a time-scale set by the scattering time. The time scales involved in the Loschmidt echo are similarly rich; it has been shown in certain regimes that the echo decays in time at a rate set by a Lyapunov exponent. At least in this case the echo and the out-of-time-order correlator are governed by similar timescales. Detailed discussion of all these considerations as well as the correspondence with experimental timescales may be found in both [22, 26].

Let us finally turn to black holes and recall some of the recent insights into their chaotic properties [6]. As discussed briefly in the introduction, black holes are governed by a number of different time scales. The dynamics of black holes also depend sensitively on the the asymptotic structure of spacetime. In flat space black holes eventually Hawking radiate away all their mass and evaporate. In anti de Sitter space, the case of interest to us here, black holes can remain in thermal equilibrium with their Hawking radiation (AdS acts like a box). From the perspective of the boundary field theory, the black hole is dual to an ordinary thermal state of the field theory. We will say nothing about black holes in an expanding de Sitter universe in this work.

Mirroring the discussion of many-body timescales above, the local equilibration of a black hole is given by the inverse temperature. The decay of time-ordered correlation functions is controlled by the local equilibration time or more generally by the quasi-normal modes of the black hole. These modes are properties of the entire black hole geometry, not just the horizon, and so are less universal. The global equilibration time or scrambling time is analogous to the Ehrenfest time in single particle quantum chaos. Roughly speaking, both represent

the timescale for information to spread over the available Hilbert space. For black holes in Einstein gravity the scrambling time is $\frac{1}{2\pi T}\log S_{\rm BH}$. Like the quasi-normal modes, the scrambling time is set by the inverse temperature, but unlike the quasi-normal modes it is a property of the near horizon geometry and has a universal character.

The nature of the dynamics on longer time-scales, say times of order the entropy $S_{\rm BH}$ or longer times of order the inverse level spacing $e^{S_{\rm BH}}$, depend in more detail on the nature of the full quantum state. A black hole formed from collapse corresponds to the unitary dynamics of an isolated system prepared in an initially nonequilibrium state which subsequently undergoes closed system thermalization. The system begins in some nonequilibrium state $|\psi\rangle$ with energy E_ψ above the ground state. The time evolved state

$$|\psi(t)\rangle = e^{-iHt}\,|\psi\rangle \tag{25}$$

will rapidly approach local thermal equilibrium at a temperature T_ψ determined by $E_\psi = E(T_\psi)$ where $E(T)$ is the thermodynamic energy at temperature T. Here local equilibrium means that density matrices of subsystems are close to those of the thermal equilibrium state at temperature T_ψ [59, 60].

Alternatively, the system can be initialized in a mixed state given by the canonical thermal equilibrium state $\rho = e^{-H/T}/Z$. Introducing a second copy of the system which purifies the thermal state, we can consider the thermofield double state

$$|\psi\rangle_{12} = \sum_E \sqrt{\frac{e^{-E/T}}{Z}}\,|E\rangle_1 \otimes |E\rangle_2\,. \tag{26}$$

Where as the thermal state describes a single black hole, the thermofield double state describes an entangled state of two black holes [71]. The geometry corresponds to the maximum analytic extension of a single black hole geometry and is called the eternal black hole. The two black holes in the eternal black hole geometry are connected by a wormhole or Einstein-Rosen bridge which is nontraversable. In such a state, the out-of-time-order correlations we have considered can be recast as correlations between the two sides of the black hole. As such they probe the structure of the black hole interior which connects the two sides. They are also directly related to high energy gravitational scattering experiments and to the effects of high energy shockwaves [6, 72].

Analysis of Dissipation

We have used quantum trajectories methods to simulate the effects of dissipation in the cavity QED implementation. A good introduction to quantum trajectories can be found in [73].

As discussed in the main text, the cavity implementation suffers from cavity decay at a rate κ and atomic spontaneous emission at a rate Γ. In solving for the effective dynamics of the atomic pseudo-spin states $|\uparrow\rangle_i, |\downarrow\rangle_i$, we find that these decay processes are described by a set of Lindblad jump operators L. The cavity decay is described by

$$L_\kappa = \sqrt{\mu}\; S_x, \tag{27}$$

where μ is the rate at which photons are scattered from the cavity per atom. The effect of L_κ is to diffusively smear out the wavefunction in directions perpendicular to $\hat{x}$. Written in terms of physical parameters in the cavity QED setup (Fig. 2b of main text),

$$\mu = \kappa\left(\frac{\Omega g}{\Delta\delta}\right)^2 = \frac{2\chi}{d} \tag{28}$$

where the atom-atom coupling is $\chi = \Omega^2 g^2/\Delta^2\delta$ (see Eq. 7 in main text) and we define the detuning parameter $d = 2\delta/\kappa$. Here we have assumed uniform coupling $g_\alpha(r_i) = g$, a fixed ratio between Rabi frequencies and detunings $\Omega_\downarrow(r_i)/\Delta_\downarrow = \Omega_\uparrow(r_i)/\Delta_\uparrow \equiv \Omega/\Delta$, and a large two-photon detuning $\delta \gg \kappa$. The origin of the rate μ can be understood in second-order perturbation theory: due to the two-photon transition driven by $\Omega_\downarrow, g$ (respectively $\Omega_\uparrow, g$), the cavity will be populated by a single photon with probability $(\Omega g/\Delta\delta)^2$, which will then leak from the cavity at a rate κ.

The spontaneous emission is described by a set of $4N$ jump operators:

$$\begin{aligned} L_i^+ &= \sqrt{\gamma}\;\; |\uparrow\rangle\langle\downarrow|_i \\ L_i^- &= \sqrt{\gamma}\;\; |\downarrow\rangle\langle\uparrow|_i \\ L_i^\uparrow &= \sqrt{\gamma}\;\; |\uparrow\rangle\langle\uparrow|_i \\ L_i^\downarrow &= \sqrt{\gamma}\;\; |\downarrow\rangle\langle\downarrow|_i\,, \end{aligned} \tag{29}$$

where 2γ is the spontaneous scattering rate per atom. These jump operators describe individual spin-flips (L_i^+ and L_i^-) and spin-projections ($L_i^\uparrow$ and $L_i^\downarrow$) induced by spontaneous scattering events. In terms of physical cavity parameters,

$$\gamma = \frac{\Gamma}{2}\left(\frac{\Omega}{2\Delta}\right)^2 = \frac{\chi d}{4\eta}. \tag{30}$$

This rate can also be understood in perturbation theory: the drive field $\Omega_\downarrow$ (respectively $\Omega_\uparrow$) will populate the excited state $|e\rangle$ with probability $(\Omega/2\Delta)^2$, which will subsequently decay to one of the two ground states $|\uparrow\rangle_i, |\downarrow\rangle_i$ at a rate $\Gamma/2$. From Eqs. 28 and 30 it is evident that, once the cooperativity η has been fixed, the detuning d completely controls the relative strengths of the two forms of dissipation.

The cavity jump operator L_κ acts symmetrically on the atomic ensemble and can be simulated in the $(N+1)$-dimensional Dicke subspace of the full 2^N-dimensional

Hilbert space $\mathcal{H}$. The spontaneous jump operators, however, break this symmetry and appear to require simulation of the full Hilbert space. This is obviously prohibitive for more than just a few atoms.

Fortunately, the method of quantum trajectories allows us to circumvent this problem. A single quantum trajectory consists of a known sequence of jump operators, allowing us to begin the simulation in a manageable subspace of $\mathcal{H}$ and introduce new subspaces only when they are needed. The trick is to take advantage of the following identity for the addition of angular momentum:

$$\bigotimes_{i}^{N} \mathbf{2}_i = \bigoplus_{P,j} \mathbf{P}_j \tag{31}$$

where $\mathbf{P}_i$ denotes the Hilbert space of a spin-$(P-1)/2$ particle and the sum over j labels the different copies of a given spin-P. For instance, for $N = 2$ this gives the familiar decomposition of a pair of spin-1/2 particles into singlet and triplet subspaces: $\mathbf{2} \otimes \mathbf{2} = \mathbf{3} \oplus \mathbf{1}$. The key observation is that each spontaneous jump operator causes transitions *between* the subspaces $\mathbf{P}_j$, while the unitary dynamics and cavity decay move the state vector around *within* these subspaces. By organizing $\mathcal{H}$ into a collection of Dicke subspaces, we can evolve the state vector in only the relevant subspaces, and introduce new subspaces only when we apply a spontaneous jump operator.

The number of subspaces $\mathbf{P}_j$ required doubles for each spontaneously emitted photon, so despite significant gains from using subspaces efficiently the effective Hilbert space becomes prohibitively large after only a few scattering events. We therefore restrict our simulations to the first five spontaneously emitted photons. There is no such restriction on the number of photons scattered from the cavity.

In this paper, we have assumed that all rotations (including controlled rotations) occur instantaneously and without dissipation. The dissipation enters the dynamics only through the S_x^2 evolution.

Conditions on the Cooperativity

Here we derive some estimates involving the cooperativity η that are mentioned in the main text. Namely, we derive the estimated maximum controlled phase angle of order $\sqrt{\eta/N}$, and the requirement that $\eta > (k \ln N)^2$ in order to observe chaotic timescales.

Although we assume unitary controlled rotations in our simulations, in reality these controlled operations will be compromised by dissipative effects. To understand the details of this, we must specify exactly how to achieve controlled rotations in the cavity scheme. First we coherently convert the control qubit state into a cavity photon state via stimulated Raman adiabatic passage [74]. Then, if we design a cavity whose resonance frequency lies at

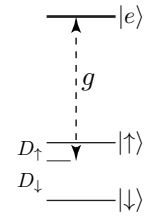

FIG. 5.

detunings $D_\uparrow, D_\downarrow$ from the two ensemble ground states $|\uparrow\rangle_i, |\downarrow\rangle_i$ as shown in Fig. 5, the interactions between the atoms and the cavity result in the effective Hamiltonian [75]

$$H = -\xi\, a^\dagger a S_z, \tag{32}$$

where $\xi = 2g^2/D$, $D = 2D_\uparrow D_\downarrow / (D_\uparrow + D_\downarrow)$, and a is the cavity mode annihilation operator. This Hamiltonian applies a rotation of angle $\phi = \xi t$ about the $\hat{z}$-axis if there is a photon in the cavity, and applies the identity if there is not.

The controlled rotation operation fails, however, if we lose the photon due to cavity leakage or spontaneous emission. To ensure a low probability of failure, we therefore require the mean number of photons lost through both processes to be less than 1:

$$N\Gamma_{\rm sc} t + \kappa t < 1 \tag{33}$$

where $\Gamma_{\rm sc} = g^2\Gamma/D^2$ is the rate at which photons are lost due to spontaneous emission.

For fixed ϕ, the evolution time t determines which dissipation path dominates. Short evolution times require small detuning D in order to achieve the angle ϕ, which increases the probability of spontaneous emission. On the other hand, long evolution times increase the probability of cavity decay. We choose an optimal evolution time $t_{\rm opt}$ that makes the probability of failure (i.e. the left-hand side of Eq. 33) as low as possible:

$$t_{\rm opt} = \frac{\phi}{\kappa}\sqrt{\frac{N}{\eta}}, \tag{34}$$

which also fixes the optimal detuning $D_{\rm opt} = \sqrt{\eta N}\ \Gamma/2$. Plugging this evolution time back into Eq. 33, we see that the achievable controlled rotation angles are limited to:

$$\phi < \sqrt{\frac{\eta}{4N}}. \tag{35}$$

Moreover, the closer we are to saturating this bound, the more likely the controlled rotation operation is to fail on any given trial.

We now turn to the requirement on η necessary to observe chaotic timescales in $F(t)$. Following the arguments

in [41], we require order $\ln N$ kicks in order to observe the onset of classical chaos. During this time, cavity decay and spontaneous emission will act on the ensemble and reduce the fidelity of F.

Following arguments in [37], smearing caused by the relaxation operator L_κ causes the spin variance in directions perpendicular to $\hat{x}$ to grow like $\Delta S^2 \sim N^2\mu t$. Simultaneously, spontaneous emission events produce random spin-flips, which cause the spin variance to grow like $\Delta S^2 \sim N\gamma t$. Taking the view that spontaneous emission events are likely to be more destructive than cavity decay to the highly entangled states produced by the kicked top Hamiltonian, we conservatively limit the evolution to a single spontaneously emitted photon:

$$2N\gamma t \lesssim 1, \tag{36}$$

and allow the relaxation operator L_κ to smear the state by an amount at most equal to the spread of the initial coherent spin state:

$$N^2\mu t \lesssim N. \tag{37}$$

Written in terms of the detuning d, and fixing the minimum number of kicks necessary to observe classical chaos $N\chi t/k \sim \ln N$, these conditions are:

$$\frac{d}{2\eta}k\ln N \lesssim 1, \qquad \frac{2}{d}k\ln N \lesssim 1. \tag{38}$$

Combining these two inequalities, we obtain:

$$\eta \gtrsim \frac{d}{2}k\ln N \gtrsim (k\ln N)^2. \tag{39}$$